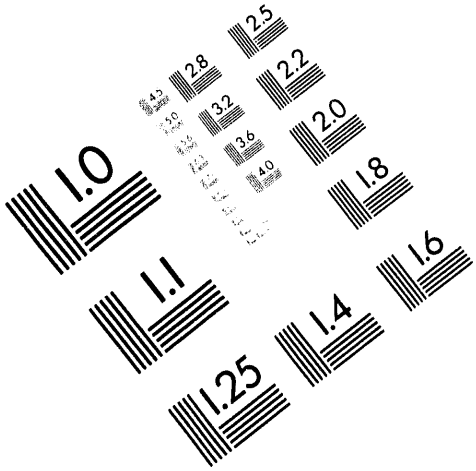

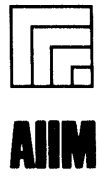

Association for Information and Image Management

1100 Wayne Avenue, Suite 1100
Silver Spring, Maryland 20910

301/587-8202

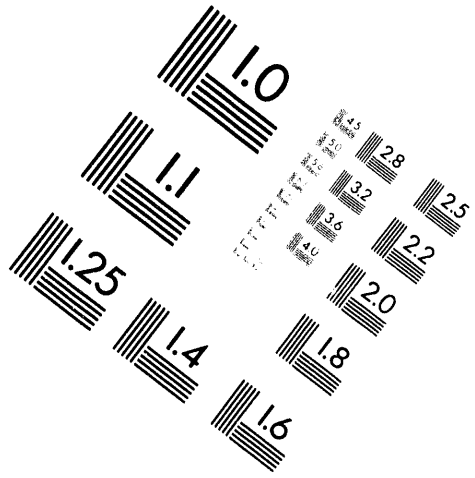

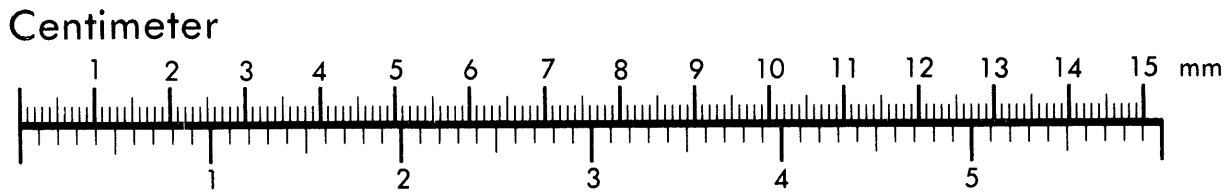

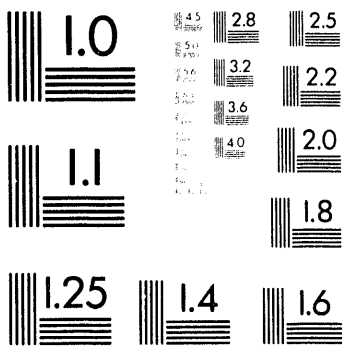

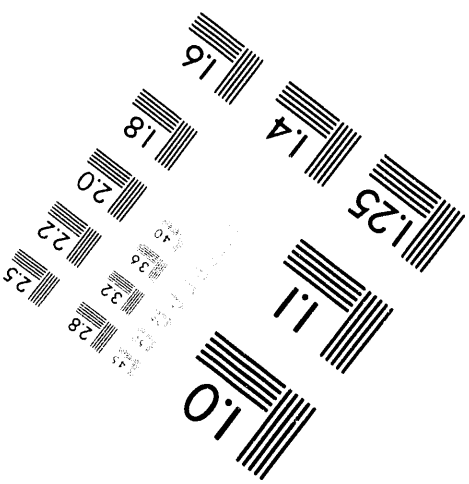

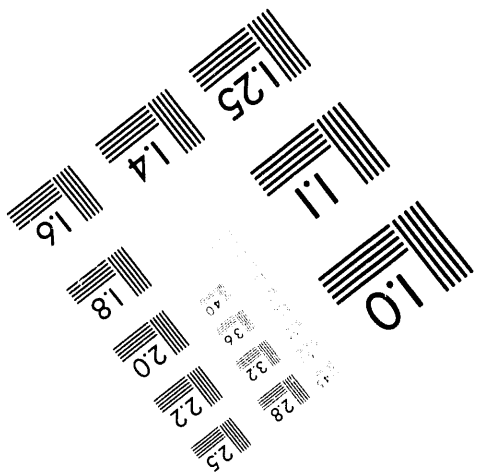

MANUFACTURED TO AIIM STANDARDS
BY APPLIED IMAGE, INC.

1 of 1

Conf-931079--23
BNL-NUREG-60148

RAMONA-4B DEVELOPMENT FOR SBWR SAFETY STUDIES *

U. S. Rohatgi, A. L. Aronson, H. S. Cheng, H. J. Khan, A. N. Mallen
Department of Advance Technology, Brookhaven National Laboratory, Upton, New York 11973

1. INTRODUCTION

The Simplified Boiling Water Reactor (SBWR) is a revolutionary design of a boiling-water reactor. The reactor is based on passive safety systems such as natural circulation, gravity flow, pressurized gas, and condensation. SBWR has no active systems, and the flow in the vessel is by natural circulation. There is a large chimney section above the core to provide a buoyancy head for natural circulation. The reactor can be shut down by either of four systems; namely, scram, Fine Motion Control Rod Drive (FMCRD), Alternate Rod Insertion (ADI), and Standby Liquid Control System (SLCS). The safety injection is by gravity drain from the Gravity Driven Cooling System (GDCS) and Suppression Pool (SP). The heat sink is through two types of heat exchangers submerged in the tank of water. These heat exchangers are the Isolation Condenser (IC) and the Passive Containment Cooling System (PCCS).

The unique design of SBWR imposes new requirements on the analytic methods for modeling its behavior. The close coupling between the power and flow, and also flow distribution among the parallel channels require a multidimensional power-prediction capability. The startup of the reactor has vapor generation and condensation taking place in the core requiring a model with a non-homogeneous, nonequilibrium, two-phase formulation. The instability at low flow/high power conditions requires modeling of the control systems and balance of plant, which has significant impact on the amplitude of the instability-induced power and flow oscillations.

The RAMONA-4B code has been developed to simulate the normal operation, reactivity transients, and to address the instability issues for SBWR. The code has a three-dimensional neutron kinetics coupled to multiple parallel-channel thermal-hydraulics. The two-phase thermal hydraulics is based on a nonhomogeneous nonequilibrium drift-flux formulation. It employs an explicit integration to solve all state equations (except for neutron kinetics) in order to predict the instability without numerical damping.

The objective of this project is to develop a Sun SPARC and IBM RISC 6000 based RAMONA-4B code for applications to SBWR safety analyses, in particular for stability and ATWS studies.

---

* This work was performed under the auspices of the U.S. Nuclear Regulatory Commission.

2. CODE IMPROVEMENTS

2.1 Steady-State Natural-Circulation Capability

The steady-state flow calculation in RAMONA-4B requires an iterative procedure to ensure equal pressure drop across the parallel core channels and to satisfy the loop momentum balance. The inner loop iterates on the core pressure drop and the outer loop iterates on the momentum balance. In the earlier version RAMONA-3B [1], the outer iteration loop is replaced by an adjustment of the jet pump head to satisfy the loop momentum balance. This simple adjustment is not applicable to an SBWR with natural circulation.

For general applicability of the code to both the natural and forced circulation, an outer iteration loop has been added to the steady-state flow calculation so that the loop momentum balance is achieved by adjusting the loss coefficient at the riser exit. This approach has worked quite well for the SBWR. However, because of the sensitivity of the thermal-hydraulic instability to the loss coefficient in the high-void region, it is recommended that the core inlet and single phase loss coefficient which supplement the two-phase losses in loop momentum equation be properly estimated.

2.2 Chimney Component

The chimney of SBWR is an additional vertical height extended from the upper plenum. It has been modeled in the RAMONA-4B code as a modified riser component, such that the total length of the riser can be divided into two parts, comprising the chimney and the separator.

The vertical height due to the riser is a one-dimensional flow path with two-phase wall friction, while the separator has its own loss-coefficient model. The upper plenum, separator, and the riser are modeled together with the assumption that there is no steam generation. The design objective of this component is to maintain a one-dimensional flow and provide required buoyancy head.

2.3 Flow-Dependent Loss Coefficients

The flow-dependent loss coefficients are important for the natural-circulation system of SBWR. The resistance due to the abrupt change in flow area and flow through orifices are functions of the Reynolds number. In RAMONA-4B, this has been accounted for by providing explicit loss coefficients for the inlet and exit of each flow segment in the form

$$f = a\,Re^{b} + c \quad ,$$

where, a, b, and c are user-specified input data on the flow-dependent loss coefficients. These values are different for laminar and turbulent flow regimes.

2.4 Isolation Condenser

Isolation Condensers (IC) are important components of the safety systems for the advanced design of SBWR by General Electric (GE). Active usage of Isolation Condensers can also be found in a few of the current operating reactors, e.g., Oyster Creek, Millstone, etc. Applications of these components include passive operation for reactor pressure regulation as well as in decay-heat removal. IC consists of a heat exchanger submerged in a pool. The heat exchanger is connected to the steam dome for steam supply and to the downcomer for the return of condensate.

The Isolation Condenser model incorporated into RAMONA-4B is based on the IC design of GE SBWR [2]. The Isolation Condenser has been modeled as a single control volume enclosing the condenser tubes with an upper and a lower plenum. The model accounts for variation in pool side heat transfer coefficient in different tubes. Transient mass and energy balance equations are used to solve for pressure and enthalpy within the control volume. Momentum change in the IC is assumed to be negligible. The governing equations for the IC model and the geometry of the IC have been reported earlier [3]. The flow inertia in the lines to and from the IC are assumed to be negligible. Therefore, they are decoupled from the transient mass and energy balance of the IC. The quasistatic momentum equations for the inlet steam line and the condensate return line determine the rate of steam inflow and condensate outflow from the IC. Steam entering the IC is assumed to be always saturated, while the liquid leaving the IC is at either subcooled or saturated condition, depending on the heat removal capacity. The initial level of liquid in the IC is a variable depending on the existing two-phase mixture state.

Heat removal from the system is dependent on the IC pool condition and the heat transfer characteristics of the IC tubes in response to the variable thermal conditions inside the tubes. Three important heat transfer mechanisms considered in this model are:

1. Turbulent film condensation heat transfer inside the multiple parallel IC tubes,

2. Heat conduction through the tube wall, and

3. Natural convection and pool boiling heat transfer between the tube external surfaces and the pool water.

2.5 Balance of Plant (BOP)

Balance-of-plant models are needed for a realistic prediction of plant transients. For the earlier version RAMONA-3B without the BOP models, it was necessary to prescribe the BOP response in a plant transient as the boundary conditions (e.g., feedwater flow and temperature). Since the boundary conditions are not known *a priori*, such an approach will contribute to the uncertainty of the predicted transient response. Furthermore, the BOP response might have a feedback effect on the large-amplitude density-wave oscillation owing to the thermal-hydraulic instability.

The BOP models [4] of the BNL Engineering Plant Analyzer (EPA) have been implemented in the RAMONA-4B code. The BOP models consist of:

1. Turbine dynamics,
2. Feedwater train dynamics,
3. Feedwater preheater dynamics,
4. Condenser dynamics.

The turbine dynamics is modeled by quasistatic mass, energy, and momentum balance. The high-pressure turbines and low-pressure turbines are lumped into a two-stage turbine, an impulse stage and a reaction stage. The inlet and exit mass flow rates of the turbines as well as the extraction steam are calculated without the flow inertia (quasistatic momentum balance). The inlet and exit turbine enthalpies are calculated in terms of the isentropic turbine enthalpy loss and a turbine efficiency.

The feedwater train dynamics is modeled by a centrifugal feedwater pump for an incompressible single-phase liquid with constant loss coefficients and friction factors. The quasi-static momentum balance is used to derive the feedwater mass flow rate and an equation of conservation of angular momentum is employed to calculate the feedwater pump speed using an input moment of inertia for the feedwater pump/turbine assembly.

The feedwater preheater dynamics is modeled by a counter-current flow heat exchanger consisting of a drain cooler and a main cooler in series. The quasistatic energy balance in the heat exchanger gives rise to the overall temperature rise of the feedwater in the preheaters, which determines the feedwater temperature.

The condenser dynamics is modeled by an equilibrium mixture of vapor and liquid water at rest. Transient mass and energy balances along with the equation of state give rise to the state equations for the condenser pressure and mixture enthalpy. These equations are integrated in time to obtain the transient response of the condenser pressure and enthalpy.

2.6 Boron Circulation in the Vessel

The boron transport model in RAMONA-3B [1] is inadequate for accurate tracking of boron in the reactor core because of the very few nodes used for boron transport. There are only ten nodes used for the reactor pressure vessel (RPV) of which three are used for the core. Furthermore, the multiple core channels are lumped into a single channel for boron tracking in the core. The strong nuclear-thermal-hydraulic coupling in a SBWR, due to the natural circulation coolant flow, requires an accurate calculation of boron concentration in the multiple parallel channels of the core. To this end, a new detailed boron transport model has been implemented in the upgraded version RAMONA-4B.

For RAMONA-4B, the boron circulation in the vessel is modeled by a local transient boron transport equation, which is integrated in time in every hydraulic cell throughout the vessel including the multiple parallel coolant channels in the core. Furthermore, the boron flow reversal can also be calculated everywhere in the vessel. These features allow the code to

predict accurately the nonuniform boron dispersion in the vessel.

In order to account for the imperfect boron mixing with the liquid water (especially at the low-flow condition), three flow-dependent boron-mixing efficiency functions have been introduced to be associated with the boron flow for the up-flow, down-flow, and horizontal flow (at lower plenum), respectively. This feature makes it possible to predict the potential boron stratification that may occur in the lower plenum at very low flow rates (less than 5% of rated core flow).

2.7 Standby Liquid Control System (SLCS)

The Standby Liquid Control System of SBWR is a backup shutdown system to be used in case of the failure of normal scram system. The system consists of an accumulator tank maintained at a high pressure, a piping system with control logic, and a high-velocity core injection system.

In RAMONA-4B, this system has been modeled as an independent component. Momentum balance between the accumulator tank and the RPV injection port is used to determine the flow rate of boron solution from the tank. The initial conditions inside the tank are user specified, which include the cover-gas pressure, solution density, liquid level within the tank, and other geometric and initialization data. Polytropic expansion of the cover gas is assumed to determine the transient cover gas pressure in the momentum equation. The boron solution level, flow rate, and void fraction as a function of time are also calculated.

The transient boron flow rate is used as the boron injection rate to the boron transport model for calculating local boron concentrations, which in turn provide input to neutron kinetics for boron reactivity calculation. The SLCS can be activated either automatically or manually. The automatic SLCS actuation is initiated by high-pressure and low-level setpoints. Delays in the control logic and valve operation are taken into account in accordance with the actual system specification.

3. DEVELOPMENTAL ASSESSMENTS

3.1 Calculational Model

RAMONA-4B is a detailed best-estimate thermal-hydraulics computer code with 3D neutron kinetics, capable of modeling a full core with 800 neutronic channels and 200 thermal-hydraulic channels along with 24 axial cells. The hydraulic model is based on nonequilibrium drift-flux formulation for two-phase flow with provision for flow reversal [4]. The neutronic model is based on a well-established 1½-group diffusion theory [1]. The three-dimensional neutron kinetics is an important feature of the calculational model described below. RAMONA-4B has a separate section to generate a steady-state condition. This section uses the same formulation as the transient section.

The RAMONA-4B calculational model used in the present assessment is shown in Figure 1. It includes the reactor pressure vessel with all important internal components (reactor core,

upper plenum and riser, steam separator and dryer, steam dome, downcomer, lower plenum, and jet pumps) and the recirculation loops, steam lines and control systems. The reactor core is modeled with 101 neutronic channels and 25 thermal-hydraulic channels assuming eighth-core symmetry as shown in Figure 2. Twenty-four axial cells are used in each of the multiple core channels in order to obtain accurate axial power and void distributions.

The nuclear parameters for the 3D neutron kinetics correspond to Browns Ferry Unit 3, a typical BWR4. The cross sections and their feedback coefficients were generated to represent the end of cycle 5 (8766 MWD/MTU). The three-dimensional exposure and the history-dependent void distributions were taken into account using the auxiliary code BLEND [5] to produce 77 sets of cross sections and the corresponding feedback coefficients. These cross section sets have been used to predict both the radial and axial power distributions in very good agreement with the Browns Ferry-3 cycle-5 measurements [6].

3.2 SBWR Natural Circulation Steady State

As an assessment of the natural circulation steady-state capability for the SBWR, a null transient from hot-full-power conditions was run for 500 seconds to see if a steady state would hold in the long run. That this is indeed the case and is demonstrated in the null transient results in Figures 3 through 6 for the core flow, reactor power, system pressure, steam flow, and feedwater flow, respectively.

We conclude that the double-loop iteration algorithm described in Section 2.1 does work well for SBWR.

3.3 Isolation-Condenser Performance

The effectiveness of ICs will be measured by their influence on the frequency of operation of the Safety and Relief Valves (SRVs) for overpressure protection. In the SBWR, the Emergency Core Cooling System (ECCS) has been replaced by a passive system, eliminating the High Pressure Core Injection (HPCI) and Reactor Core Isolation Cooling (RCIC) systems. Thus, the reactor performance, with operating ICs, will be investigated in the absence of these components.

3.3.1 Transient Description

The transient considered here is an ATWS event initiated by the closure of all four MSIVs in four steam lines within 4 seconds with postulated scram failure. This will result in a sharp rise in the vessel pressure, which leads to a large power increase due to void collapse. The SRVs will open at their upper pressure setpoints and will close at their lower pressure setpoints. Thus, after the initial part of the transient, the cyclic operation of the SRVs will control the reactor pressure. Early shutdown of the incoming feedwater flow will cause a decrease in the collapsed water level, which will initiate the HPCI, at the low water level setpoint in the case of regular BWRs. The ICs will be activated by either a 10% closing of the MSIV or exceeding a pressure setpoint of 7.9 MPa.

A regular BWR operating without any isolation condenser has been used as the base case for comparison of the results. Several modifications in the input of the base case have created other significant cases of interest. Table 1 shows the test matrix used to investigate separate effects in each case. Cases 1 and 2 refer to a BWR operating without any IC and with one IC, respectively. Cases 3 and 4 refer to transients with 1 and 3 ICs operating without HPCI respectively. Lastly, cases 5 and 6 study the effect of isolation condenser on a natural circulation system achieved by removing the recirculation pump system. The last two cases refer to a regular BWR operating without any IC and with one IC but in the absence of HPCI.

Table 1. Test Matrix for MSIV Closure

Case No.	Number of ICs	HPCI	Recirc. Pump	Observation
1	0	Active	Active	Base Case
2	1	Active	Active	Effect of IC
3	1	Inactive	Active	Effect of HPCI
4	3	Inactive	Active	Effect of ICs
5	0	Active	Inactive	Natural Circulation
6	1	Active	Inactive	Effect of IC

3.3.2 Results and Discussions

The results will be separated into two parts. In the first part we focus on the forced-circulation system, while the second part is related to the natural circulation system.

Effects on Forced Circulation System

Figure 7(a), 7(b), 7(c) and 7(d) show the transient pressure response for cases 1 through 4, respectively. The MSIV closure results in a rapid increase of the RPV pressure to 8.9 MPa within the first 10 seconds. During this period all the SRV banks have reached their relief pressures, and therefore opened sequentially. Consequent release of steam has resulted in a decrease of reactor pressure after attaining the peak pressure of 8.9 MPa. This peak pressure has remained nearly the same for all four cases analyzed. A periodic behavior of the transient pressure can be observed following the initial peak. According to the SRV pressure setpoints, the SRV bank 3 is periodically opening and closing to produce this behavior. The SRV banks 1 and 2 are open for the entire period of the transient, while the valves in bank 4 has closed within the first 20 seconds.

The cyclic frequency of the SRV operation is reduced when an active isolation condenser is used in case 2, where one IC is operating in the presence of HPCI. However, the effect of

IC is reduced after 90 seconds, as seen from Figure 7 (a) and 7(b). This is due to the actuation of HPCI, as initiated by the low level in the vessel at 45 seconds. From Figure 8(a), we see that the HPCI supplies a constant flow of 369 kg/sec during the rest of the transient. Figure 8(b) shows the combined mass flow rate of the feedwater, HPCI flow, and the condensate flow returning from the IC. The feedwater flow reduces rapidly within the first 5 seconds, as a result of the extraction steam cutoff by the MSIV closure, which has been prescribed here as an input boundary condition. The condensate return from the IC depends on several factors, including the system pressure, IC pressure, IC cooling capacity, and the liquid levels inside the downcomer and IC [3]. The resulting flow of condensate is shown to fluctuate around 30 kg/sec.

The external makeup water to the reactor vessel is largely dominated by the HPCI flow rate. Therefore, after the activation of the HPCI, the effect of the IC is negligible. According to Figure 8(b), there is no net inflow between 25 to 42 seconds. During this period, the IC activation conditions are satisfied, but the momentum balance between the IC and the condensate return port has prevented any down flow of the liquid. Figure 8(b) shows that the HPCI activation has been delayed by 20 seconds due to the operation of the IC. This delay was caused by the slower drop of the collapsed liquid level during the transient.

In the new design of SBWR, the ECCS systems are not available in the present form. In order to eliminate the effect of HPCI, cases 3 and 4 are presented, which include one and three active ICs respectively. According to Figures 8(c) and 8(d), the effect of removing the HPCI has resulted in much reduced cycling of the SRVs, although the system pressure is maintained within the same range. It is also observed that increasing the number of ICs has reduced the cycling frequency further.

The periodicity of the pressure behavior is directly related to the steam flow response shown in Figures 8(a) through 11. As a consequence of the pressure rise to 8.9 MPa in the first 5 seconds, there is a core wide collapse of voids. Because of the effect of negative void reactivity feedback, the core thermal power increased during the first 5 seconds. These processes reverse later when the system pressure is reduced, causing the void fraction to increase and resulting in a decrease in the core thermal power within 40 seconds. The periodic behavior during the transient is also evident from the void fraction and thermal power responses. Removal of the HPCI has resulted in much fewer peaks in Case 3 and 4. Therefore, the ICs are more effective in the absence of HPCI, which is the case of the SBWR design.

The effectiveness of the IC as a passive pressure regulating component has thus been demonstrated. The HPCI is initiated by the low collapsed liquid level of -1.485 meter below the entrance of the downcomer. The condensate return flow from the IC changed the transient response of the collapsed liquid level. As seen from Figures 8 and 9, the HPCI initiation by the low level setpoint has been delayed from 42 seconds to 62 seconds by the operating IC.

The condensate return to the reactor vessel from the IC is closely related to the system pressure. After the initial fluctuation in the early transient, the flow rate has stabilized at approximately 30 kg/sec. The periodicity of system pressure has resulted in fluctuation of the liquid return flow by 5 kg/sec.

Effects on Natural-Circulation System

The effects of ICs on the forced-circulation system of regular BWRs was presented in the previous section. The overall effect on a natural circulation system is quite similar to that on a forced circulation. Because of the inherent nature of the natural-circulation system, the response time is longer, which results in relatively smoother transient responses for Case 5 and 6. Figures 12(a) and 13(b) show the transient pressure responses for these cases with inactivated recirculation pumps.

The total reactor power for these cases has been reduced to 1600 MW, and the initial core flow rate is 800 kg/sec. The feedwater flow is given as a boundary condition, such that it shuts down in 3.5 seconds, while the HPCI activates on the low water level indicated earlier.

Because of the reduced power in the natural circulation system, the peak pressure observed in this transient is only 7.9 MPa, as compared to 8.9 MPa in the forced circulation cases. This peak pressure is below the operation set points for the SRVs in banks 2 and 4. Therefore, the total number of SRVs active in this natural circulation system is reduced by half. The periodic behavior of the pressure is due to the repeated opening and closing of SRV bank 3, while SRV bank 1 remains open throughout the transient. According to Figures 12 and 13, the cyclic frequency of operation for the SRVs has been reduced significantly by the use of one Isolation Condenser. The steam flow rate in the steam line also shows the periodic behavior. Figures 14 and 15 show the core thermal power during the transient. As compared to the forced circulation cases, the amplitude of oscillations during the first 40 seconds of the transient is higher. The presence of one IC has reduced the thermal fluctuations during the transient as shown in Figure 15.

3.3.3 Conclusions

The effectiveness of ICs as a pressure regulation system has been demonstrated. The cyclic frequency of opening and closing of the SRVs is reduced by the active use of the ICs. In the absence of the HPCI, the SRV operational frequency is further reduced. Hence, the effect of IC is minimal in the case of simultaneous operation of the IC and HPCI. The mass flow rate from HPCI dominates the transient response. This is an important observation for the SBWR since the effectiveness of the IC can not be fully realized in the presence of HPCI. The ECCS of the SBWR uses a passive system operating at low pressure, and high-pressure injection of liquid is prevented. Therefore, the benefit from the ICs as a pressure-regulating device is maximized in this configuration.

In the case of a natural circulation system, simulating a SBWR configuration, the effectiveness of the IC as a pressure-regulating device has also been demonstrated. In this case, the amplitude of pressure oscillations is similar to that for the forced-circulation system, although the initial peak pressure is reduced owing to the lower core thermal power of the natural circulation system. Therefore, the total number of operating SRVs is fewer than for the forced-flow case. The oscillations noted in the transient thermal power are of higher amplitudes than the previous cases. The effect of the IC is to reduce such amplitudes. The response time in the natural-circulation system is, in general, longer than that for the forced-circulation system.

Therefore, the transient events are expected to develop over a more extended time period.

3.4 Instability Due To Recirculation Pump Trip with BOP

To assess the capability of RAMONA-4B to predict thermal-hydraulic instability, a dual-recirculation-pump-trip event was simulated for a BWR4.

3.4.1 Event Description

The scenario selected for the present analysis is a two-recirculation-pump trip initiated from 100% core power and 75% core flow on the Maximum Extended Operating Domain (MEOD) rod line with postulated scram failure (ATWS) as described in Reference 3. This selection was based on the fact that a significant fraction of BWR instability events have resulted from an inadvertent recirculation pump trip (RPT).

The ATWS event initiated from the high-power and low-flow condition by inadvertent trip of both recirculation pumps is ideal for studying the density-wave oscillation characteristics because the dual RPT results in core flow reduction to natural circulation and a corresponding decrease in core power owing to increased vapor generation. This event takes the reactor into the region of power/flow map, which is more susceptible to instability as illustrated in Figure 16. Table 2 summarizes the sequence of events for the dual RPT event as calculated by RAMONA-4B.

Table 2

Sequence of Events for Two-Recirculation-Pump-Trip Event

Time (s)	Event/Action
0.0	Reactor operating at 100% power and 75% flow, both recirculation pump trip, and scram system fails.
30.0	Core flow coasts down to natural circulation, core power decreases to about 48% of rated.
50.0	Density-wave oscillations begin, core flow and core power start to oscillate.
80.0	Core power oscillation reaches limit cycle with peaks of about 150% of rated.
146.0	Core power reaches a maximum of 265% of rated.
200.0	Transient terminated.

The thermal-hydraulic inputs for the present analysis were selected to be similar to the LaSalle-2 instability event [7] of March 9, 1988. However, the initial condition is more bounding at 100% power and 75% flow than that of the LaSalle-2 event (85% power and 75% flow). This initial condition is more susceptible to density wave oscillations, and produced a critical reactor with a bottom-peaked axial power distribution as shown in Figure 17.

Feedwater flow and temperature were imposed as time-dependent boundary conditions. The time-dependent behavior of feedwater flow was taken from the TRACG analysis [8], and that of feedwater temperature was selected in such a way as to match the TRACG calculated core inlet subcooling as close as possible. The time-dependent boundary conditions of the feedwater flow and temperature are presented in Figures 18 and 19, respectively.

3.4.2 Results of Calculations

The event begins with a trip of both recirculation pumps at time zero. The RPT reduces the core flow to natural circulation (about 29% of rated) within 30 seconds as shown in Figure 20. As a result, core power is reduced from its initial rated value to approximately 50% of rated value due to increased vapor generation as shown in Figure 21. The evidence of instability is visible within one minute of the RPT event in the oscillatory behavior of both core flow and core power when the core inlet subcooling has increased beyond 18 °C as shown in Figure 22. The oscillations reached a limit cycle after approximately 80 seconds. Figure 23 presents the oscillatory behavior of core average void fraction, which demonstrates clearly that this is a density-wave oscillation.

The large-amplitude oscillations are often characterized by flow reversal in some coolant channels as is evident in the reversed flow behavior in channel 11 in Figure 24.

The system pressure response and steam flow behavior are shown in Figures 25 and 26, respectively. Because of the rapid reduction of feedwater flow at the beginning of the transient, the system pressure decreases initially and settles at about 6.75 MPa after 20 seconds. The oscillation also appears in both the system pressure and steam flow rate response through the vapor generation.

Figures 27 and 28 show the inlet and outlet flow rates for two hydraulic channels, 17 and 23. These channels represent a single rod bundle. Channel 17 is a low-power channel as it is in the vicinity of a control rod. The inlet and outlet flow rates for this channel are in phase indicating that channel is in stable mode. The high-power channel 23, on the other hand, has inlet and outlet flow rates out-of-phase and, therefore, is in an unstable mode. The parallel-channel phenomena are more evident from Figure 29 which shows that the inlet flow rates for these two channels are out of phase. These results indicate that there are out-of-phase flow oscillations taking place in the reactor core.

3.4.3 Discussion of Results

The limit-cycle oscillations in core flow and core power as calculated by RAMONA-4B exhibit the same characteristics as those calculated by TRACG [8]. However, TRACG predicts higher amplitudes than RAMONA-4B owing to different neutronic conditions and core inlet subcooling. These differences can be deduced from the reactor condition at the time of natural circulation prior to the initiation of the instability as shown in Table 3.

Table 3

Comparison of RAMONA-4B and TRACG Results before the Instability

Item	Time	RAMONA-4B	TRACG
Initial Axial Power Peaking	0 s	1.26	1.34
Core Flow	40 s	29%	30%
Core Power	40 s	50%	60%
Inlet Subcooling	40 s	13 °C	13 °C

The amplitude of the oscillations strongly depends upon the core inlet subcooling. The higher the core inlet subcooling, the stronger is the reactivity feedback. The core inlet subcooling is controlled by the feedwater temperature. The feedwater temperature during the transient was not available from the TRACG report [8]. However, in our calculations, the feedwater temperature was entered as a time-dependent boundary condition and an attempt was made to match the core inlet subcooling with the TRACG prediction as closely as possible. RAMONA-4B predicted an increase in the amplitude of the reactor power with the increase in the subcooling until the feedwater temperature and the core inlet subcooling stabilized.

During the limit-cycle oscillations, TRACG predicted a maximum amplitude of the core power of 400% (See Figure 30, taken from Ref. 8), while RAMONA-4B predicted a maximum amplitude of 265% (See Figure 18). This difference in the amplitude is generally due to the differences in core inlet subcooling, axial power profile and reactivity feedback; especially void feedback. In order to eliminate the effect of core inlet subcooling, the amplitudes from the two calculations were compared at the same inlet subcooling. TRACG predicted a subcooling of 20°C at 110 seconds and the relative power at this time was 160% as shown in Figure 30. RAMONA-4B predicted 20°C subcooling at 100 seconds and the relative power at this time was 155% as shown in Figure 21. Therefore, it is concluded that the differences in the two calculations are due to the parameters in core model such as axial profile and reactivity feedback.

The initial axial power distribution calculated by TRACG is more bottom peaked (1.34) than that by RAMONA-4B (1.26) because of the difference in the initial core conditions. In

general, a more bottom-peaked power shape will produce a higher amplitude of oscillations.

The void coefficients of cross-section sets used by TRACG are probably more negative than those used by RAMONA-4B. This is confirmed from a comparison of relative powers predicted by two codes at 40 seconds as shown in Table 3. While the flow rates and core inlet subcooling are the same, the TRACG predicted higher power than RAMONA-4B. This comparison indicates that the reactivity feedback were higher in the TRACG calculation than in the RAMONA-4B calculation. The TRACG calculation was intended as a bounding calculation to envelope GE's fleet of different BWRs. In RAMONA-4B calculation, we determined the overall void reactivity coefficient by perturbing the void profile alone from two separate steady-state calculations. The estimated void reactivity coefficient for the core used in the present analysis is -0.00055 $\delta k/k/\%$void, or -10¢/%void with an effective delayed-neutron fraction of 0.00546.

Figure 31 shows the maximum clad temperature in the core. The hot spot does exceed 1200 °C at 140 seconds. There is a possibility of clad damage at the hot spot in the core.

There are significant differences in the nodalization detail of the core between the RAMONA-4B and TRACG calculations. RAMONA-4B used 25 thermal-hydraulic channels, while TRACG used only 10 coolant channels. However, TRACG used 40 cells for each channel, placing many more cells between the bottom of the core and the first spacer grid; whereas RAMONA-4B used 24 cells with equal spacing. The effect of such different nodalization schemes is difficult to assess, and can only be resolved by a sensitivity study.

3.4.4 Summary and Conclusions

A two-recirculation-pump-trip event as defined by General Electric for their TRACG calculations has been used to assess the RAMONA-4B capability for predicting the density-wave oscillation induced by thermal-hydraulic instabilities in a BWR. The RAMONA-4B results were similar to those from TRACG calculations.

The results led us to conclude that a high-power and low-flow initial condition will most likely lead to core-wide density-wave oscillations after tripping both recirculation pumps, and that the RAMONA-4B is capable of predicting thermal-hydraulically-induced instabilities in a BWR. Furthermore, as the instability occurred during the natural-circulation mode, the calculation demonstrated the capability of RAMONA-4B code to model the SBWR.

The analysis also indicated that there is a possibility that in some of the nodes in the core, the clad temperature will exceed 1200 °C and will probably lead to some clad damage.

3.5 Loss-of-Feedwater Heating ATWS with FMCRD

3.5.1 Transient Description

The transient selected for this assessment is an ATWS event induced by the loss-of-feedwater heating together with the failure of the normal scram system. The loss-of-feedwater

heating can be caused by either of the two ways: (1) the steam extraction line to the heater is closed, and (2) feedwater is bypassed around the heaters. The total number of unavailable feedwater heaters determines the net loss of heating. In the SBWR the maximum reduction in feedwater temperature is limited to 55.6 °C. The loss of feedwater heating will result in an increase in core inlet subcooling. This will lead to an increase in the reactor power due to the negative void reactivity feedback in the core. The thermal power increases slightly to a new equilibrium value. This transient does not activate any ATWS logic. In order to investigate the effectiveness of the new SBWR feature, fine motion control rod drive (FMCRD) run-in, it is assumed that the FMCRD run-in will be initiated manually after the loss-of-feedwater heating.

The geometric data and the setpoints are specified in accordance with the conceptual design of the GE SBWR. The core represents a regular BWR core with the Browns Ferry Unit 3 cross sections at the end of cycle 5.

3.5.2 Results of Calculations

A feedwater temperature reduction of 55.6°C was initiated at 5 seconds into the transient. As a result, the reactor condition settled to a new steady state after 75 seconds. The temperature reduction of 55.6 °C is conservative since a temperature drop of 16.7 °C indicated by the Feedwater Control System (FWCS) requires the operator to send a signal to the Selected Control Rod Run- In (SCRRI), in order to reduce core power and thereby avoid scram. The loss-of-feedwater heating transient is a slow one which can be assumed to be in quasisteady state. The normal scram system was assumed to have failed during this transient.

The loss-of-feedwater heating transient is followed by the FMCRD run in at 80 seconds, which allows slow insertion of the control rods. The reactor is able to establish a quasisteady axial power shape, and the peak cladding temperature remains within the safety limits.

The results obtained from RAMONA-4B are compared to the TRACG results as reported by GE in the SSAR. The rate of power rise in the core as predicted by RAMONA-4B is higher than that of TRACG, while the system pressure remains constant for both calculations. Figure 32 shows the transient pressure response of RAMONA-4B, where the pressure is unchanged up to 75 seconds. The loss-of-feedwater heating has resulted in an increase of the core inlet subcooling as shown in Figure 33. The inlet subcooling changed from 10.1 to 17.5 °C as shown in Figure 33. Figure 34 shows that the reactor power is raised by 13% within 80 seconds due to the increased inlet subcooling. Figure 35 indicates that the FMCRD insertion begins at 80 seconds and continues until 180 seconds for full insertion. The slow insertion of control rods results in a quasisteady power profile, which is skewed to the top of the core. Figure 32 shows that the steam flow rate has decreased to 7.5% of the rated value within 100 seconds. The pressure also reaches a new equilibrium value within 100 seconds. The time required to reach the new equilibrium is 100 seconds for RAMONA-4B, while it is 60 seconds for TRACG. The feedwater flow was shut down within 10 seconds of the FMCRD initiation, which was imposed as a boundary condition to the calculation. The hottest channel fuel temperature is within the safety limit. The peak cladding temperature was found to be limited to 296°C.

4. CONCLUSIONS

RAMONA-4B code has been upgraded to include the balance of plant and control systems along with components specific to SBWR. The code has also been made operational on workstations. This code is now available to investigate stability issues not only for the current BWRs but also for ABWR and SBWR. RAMONA-4B can also be used for reactivity transients such as a rod-drop accident as well as ATWS events.

ACKNOWLEDGEMENT

This research was performed under the auspices of the U.S. Nuclear Regulatory Commission.

5. REFERENCES

[1] W. Wulff, H. S. Cheng, D. J. Diamond, and M. Khatib-Rahbar, "A Description and Assessment of RAMONA-3B MOD.0 CYCLE 4: A Computer Code with Three-Dimensional Neutron Kinetics for BWR System Transients," NUREG/CR-3664, Brookhaven National Laboratory, Upton, New York (1984).

[2] B. S. Shiralkar, M. Alamgir, and G. M. Andersen, "Thermal Hydraulic Aspects of the SBWR Design."

[3] H. J. Khan and U. S. Rohatgi,"Performance Characterization of an Isolation Condenser of SBWR," Thermal Hydraulics Proceeding for 1992 Winter Annual Meeting of the American Nuclear Society, Chicago. Also in Vol 66, TANSAO 66 1-626 (1992).

[4] W. Wulff, H. S. Cheng, A. N. Mallen, and S. V. Lekach, "The BNL Plant Analyzer," NUREG/CR-3943, BNL-NUREG-51812, Brookhaven National Laboratory, Upton, New York (1984).

[5] L. O. Eisenhart and D. J. Diamond, "Automatic Generation of Cross Section Input for BWR Spatial Dynamics Calculations, "BNL-NUREG-28796, Brookhaven National Laboratory, (1980).

[6] J. F. Carew, D. M. Cokinos, J. G. Guppy, K. Hu, and L. Y. Neymotin, "RAMONA-3B Calculations of BWR Core-Wide and Regional Power/Flow Oscillations," Internal Memo, Brookhaven National Laboratory, December 12 (1988).

[7] W. Wulff, H. S. Cheng, A. N. Mallen, and U. S. Rohatgi, "BWR Stability Analysis with the BNL Engineering Plant Analyzer," NUREG/CR-5816, BNL-NUREG-52312, Brookhaven National Laboratory, October (1992).

[8] "ATWS Rule Issues Relative to BWR Core Thermal-Hydraulic Stability", NEDO-32047, General Electric Co., February (1992).

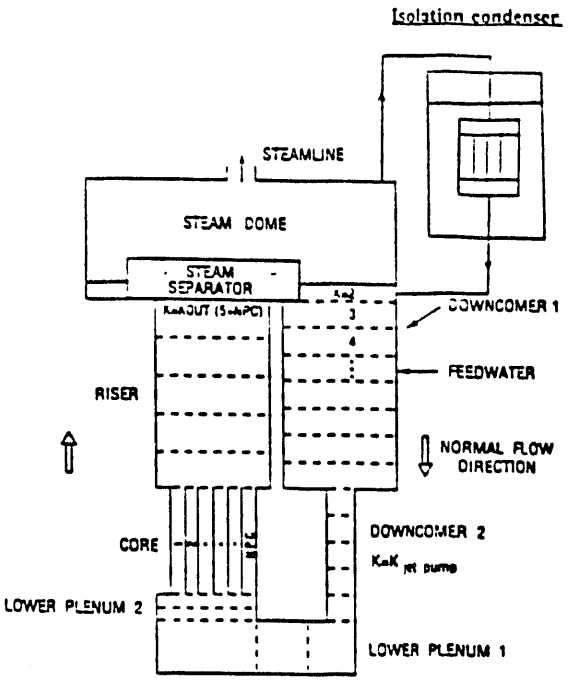

Figure 1. RAMONA-4B Nodalization

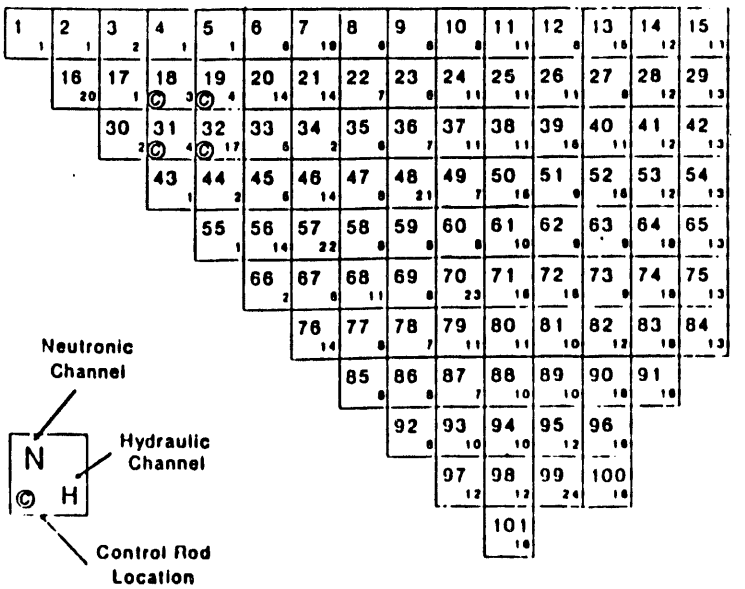

Figure 2. 1/8 Core Model for the Present Analysis

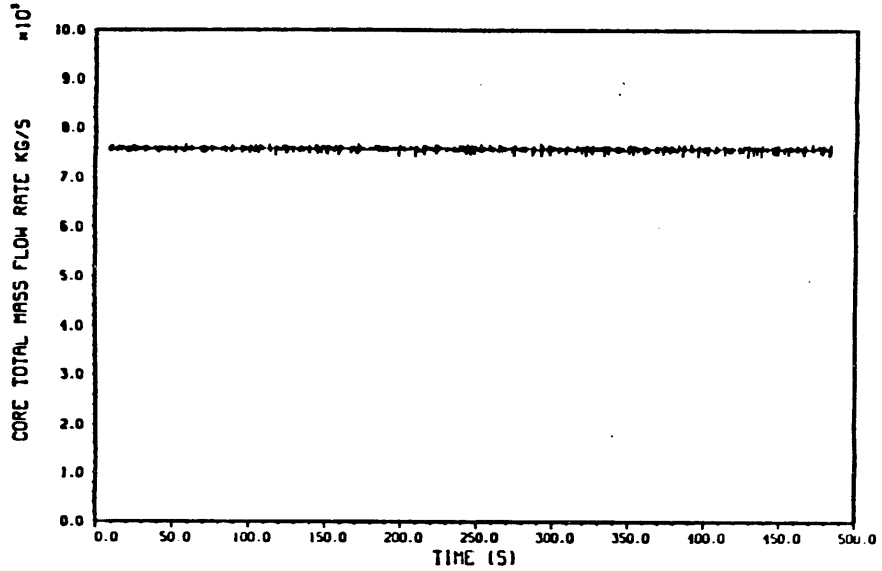

Figure 3. Core Flow Response of the Null Transient.

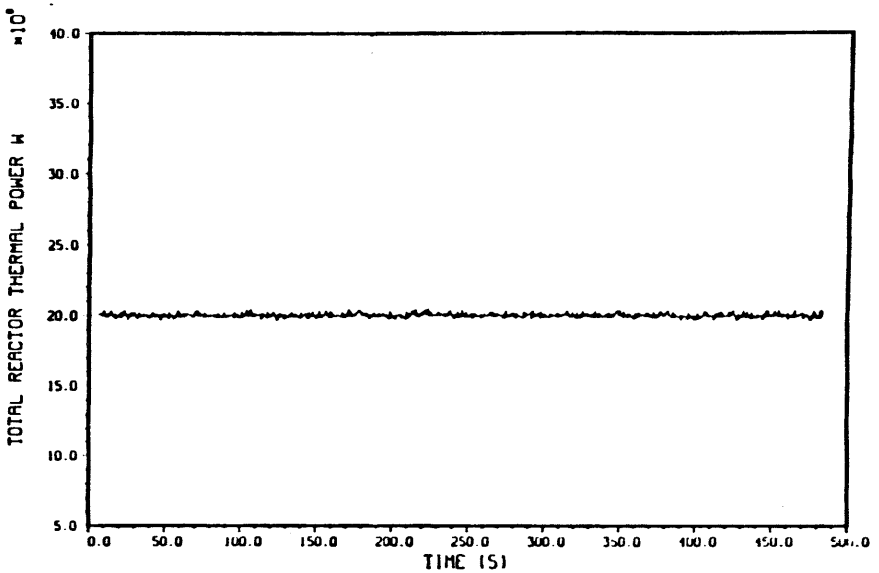

Figure 4. Core Thermal Power Response of the Null Transient.

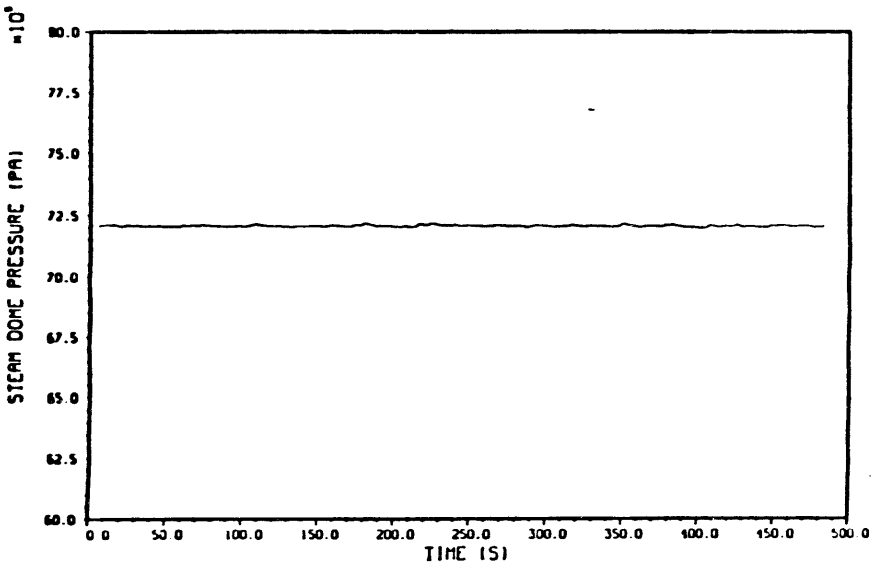

Figure 5. System Pressure Response of the Null Transient.

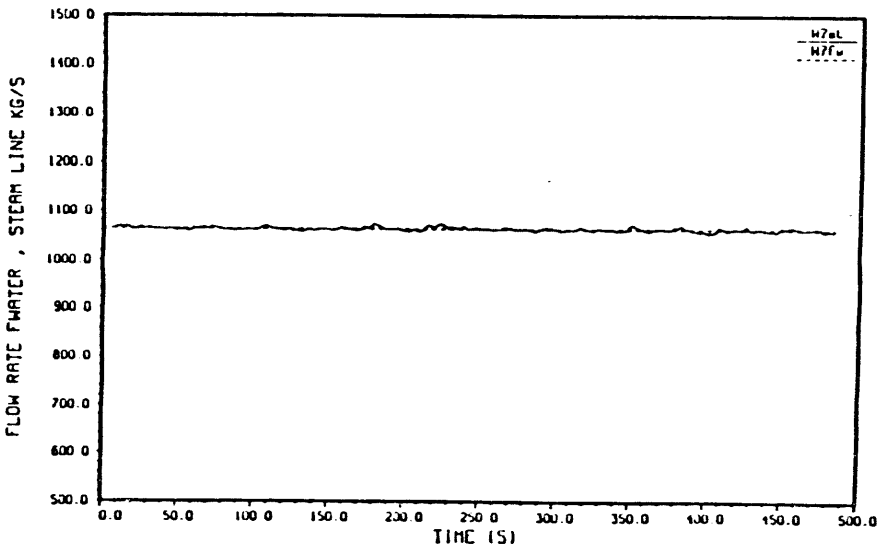

Figure 6. Feedwater and Steam Flow Response of the Null Transient.

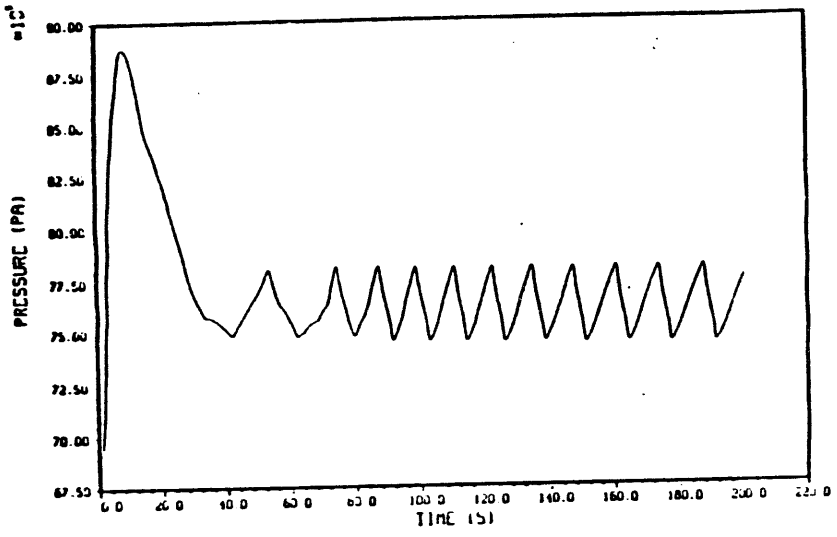

Figure 7 (a) Transient Pressure Profile for case 1

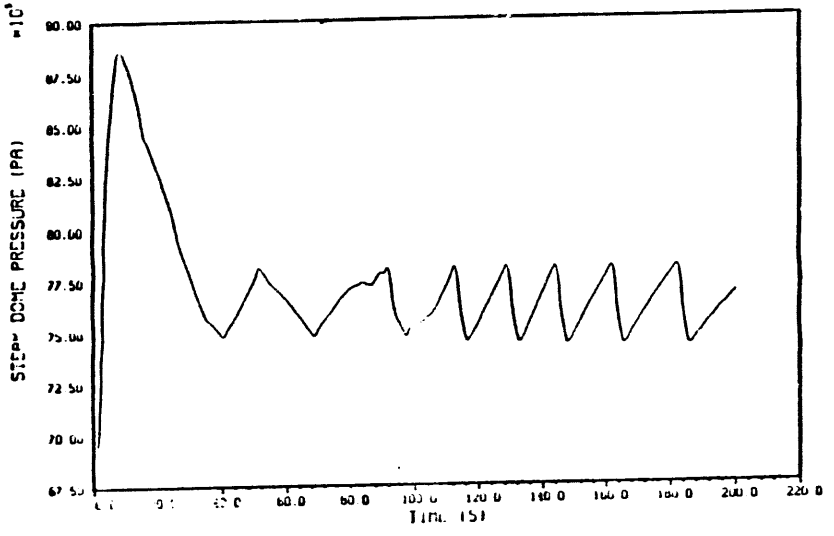

Figure 7 (b) Transient Pressure Profile for case 2

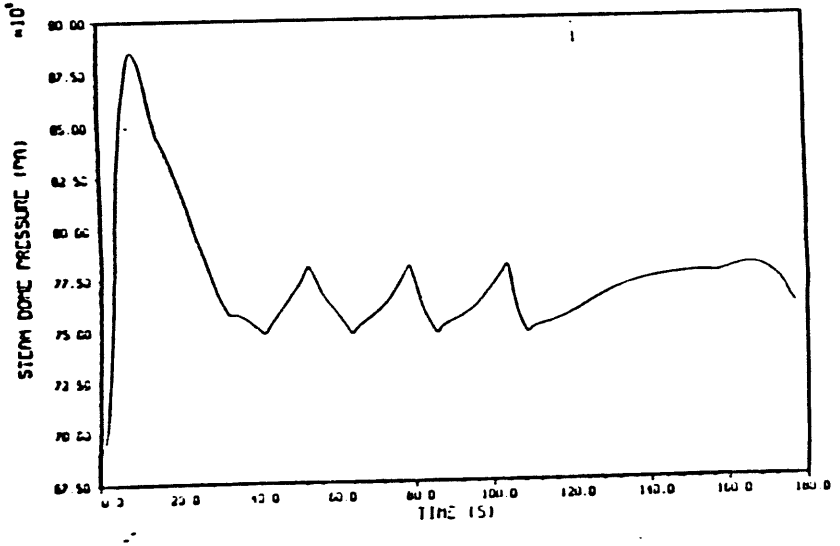

Figure 7 (c) Transient Pressure Profile for case 3

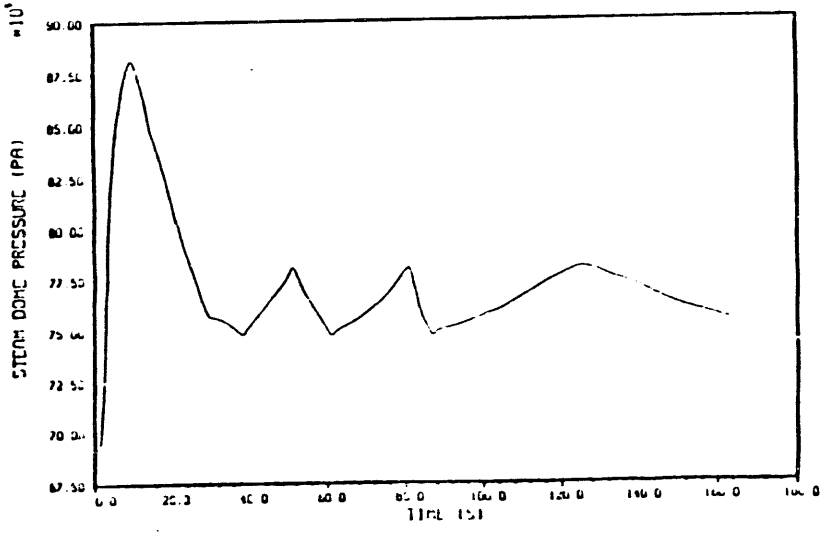

Figure 7 (d) Transient Pressure Profile for case 4

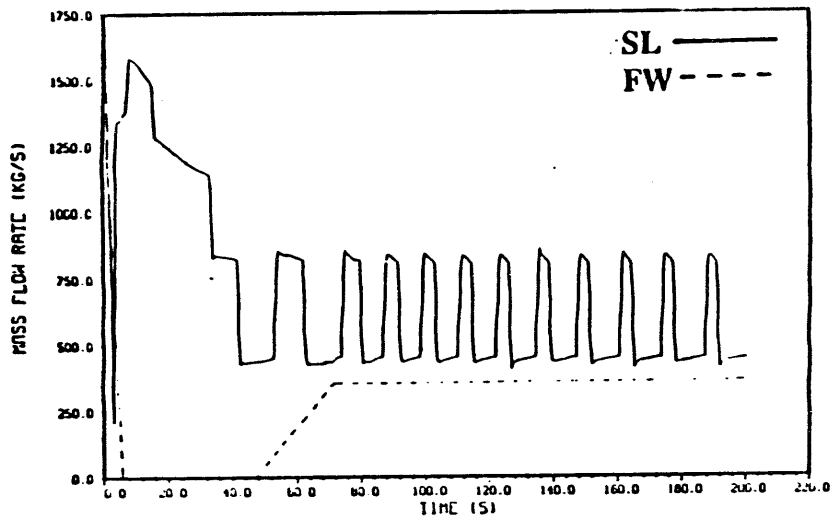

Figure 8 Steam & Feed Water Flow Rate for case 1

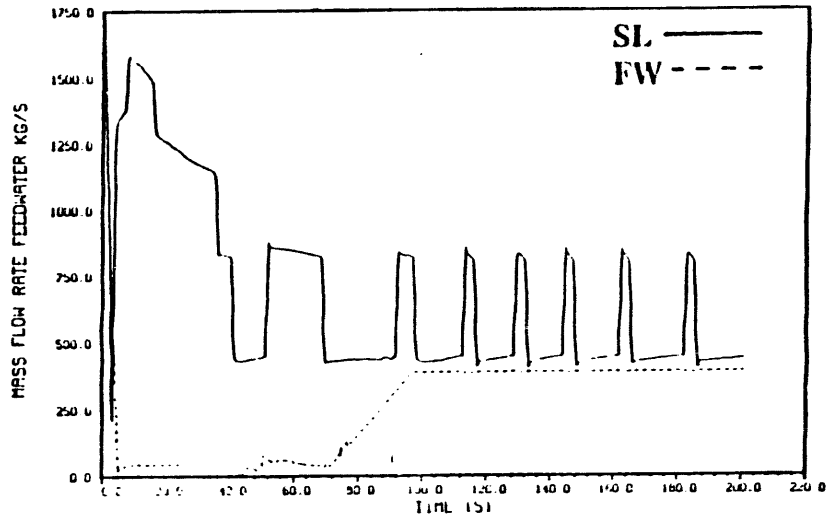

Figure 9 Steam & Feed Water Flow Rate for case 2

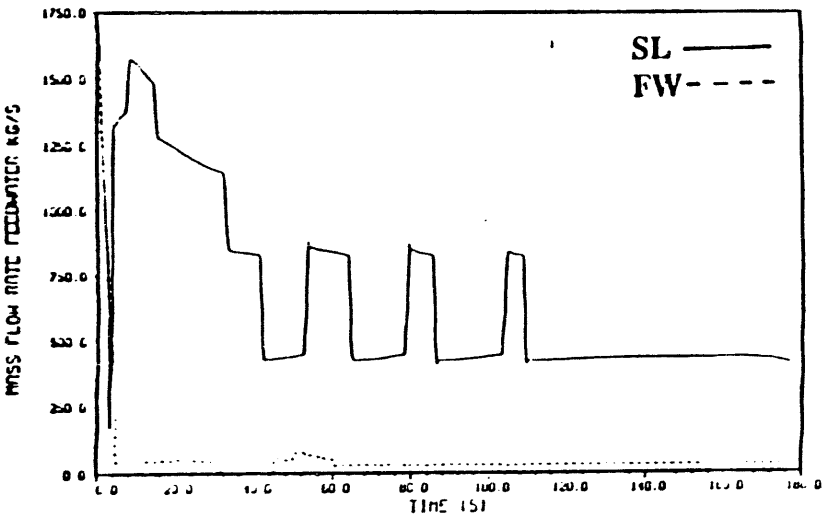

Figure 10 Steam & Feed Water Flow Rate for case 3

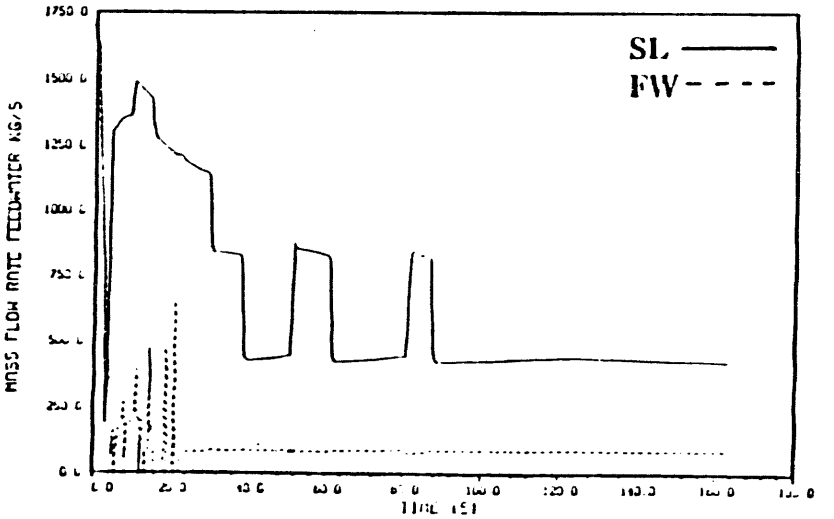

Figure 11 Steam & Feed Water Flow Rate for case 4

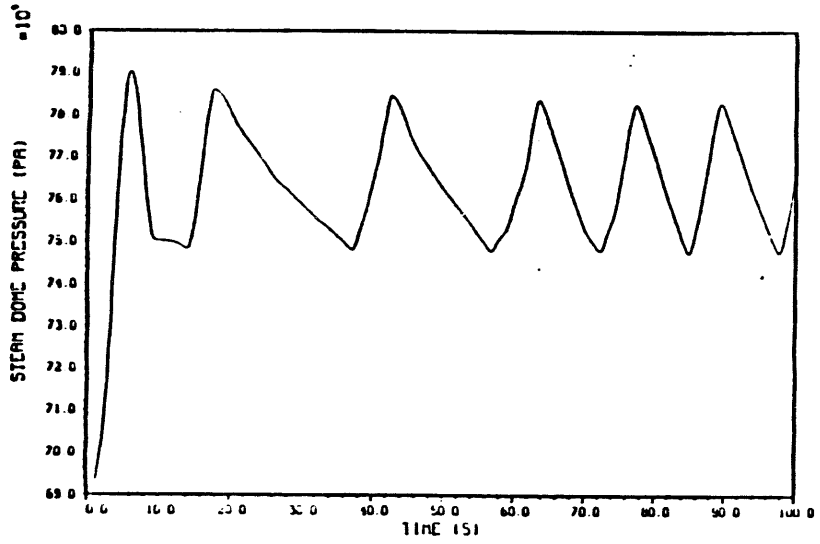

Figure 12 Transient Pressure Profile for Natural Convection Without Isolation Condenser (case 5)

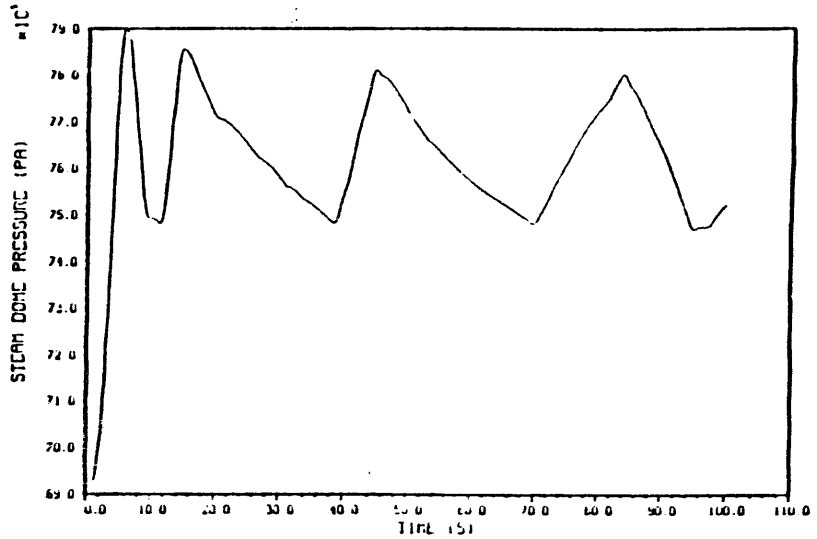

Figure 13 Transient Pressure Profile for Natural Convection With Isolation Condenser (case 6)

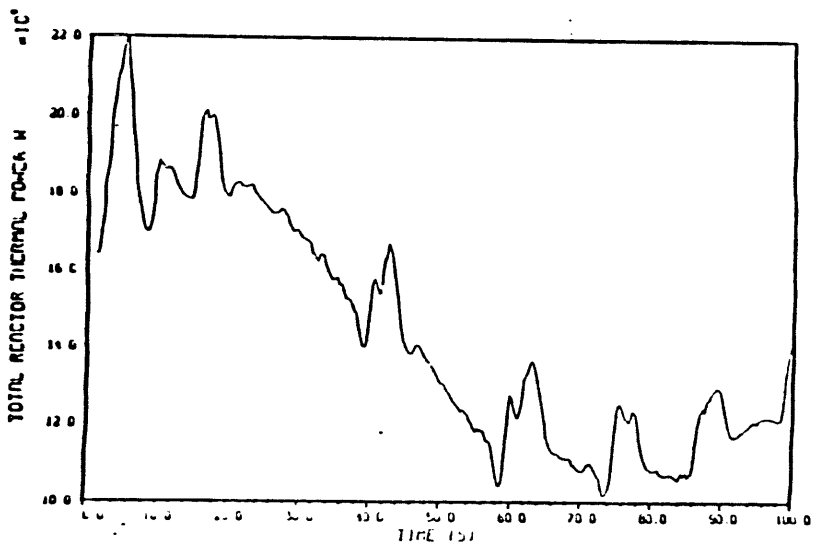

Figure 14 Thermal Power Profile for Natural Convection (case 5)

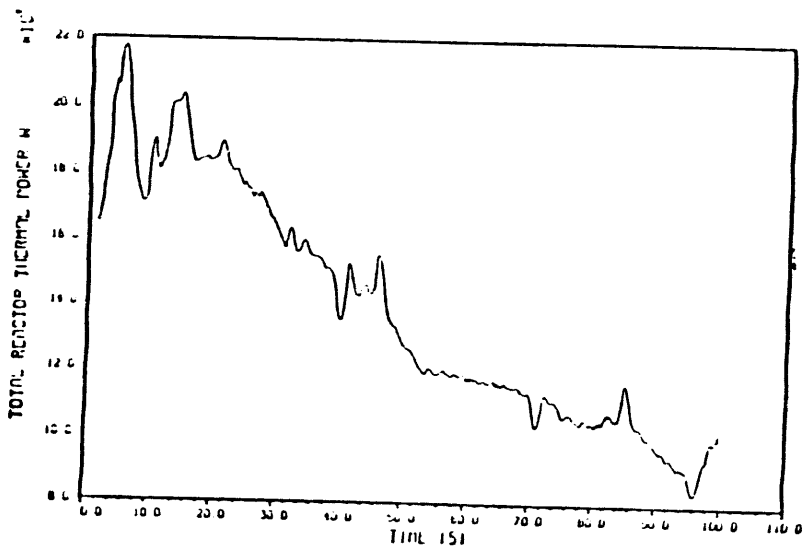

Figure 15 Thermal Power Profile for Natural Convection (case 6)

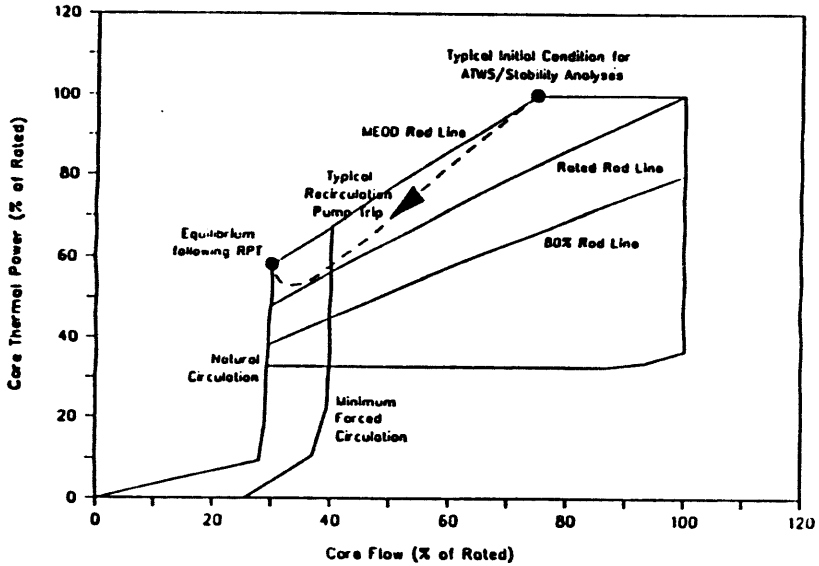

Figure 16. Typical Core Power/Flow Map of a BWR.

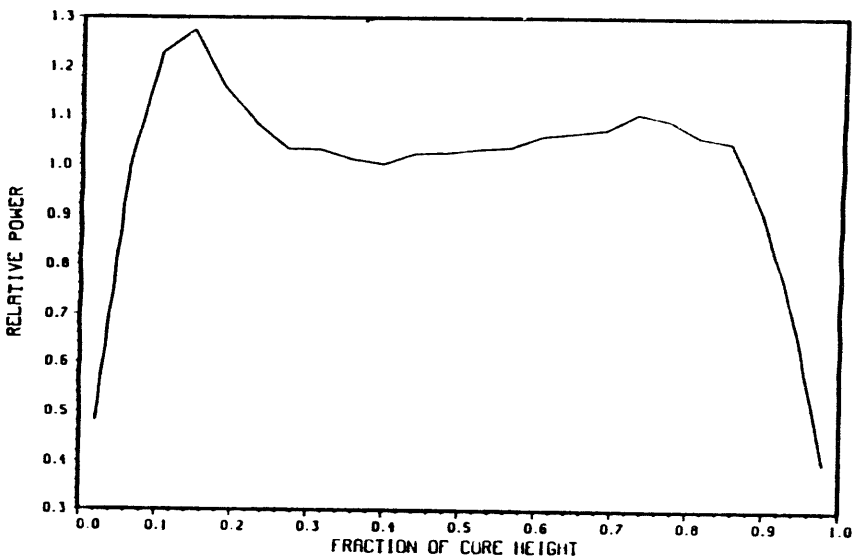

Figure 17. Initial Core Average Axial Power Profile.

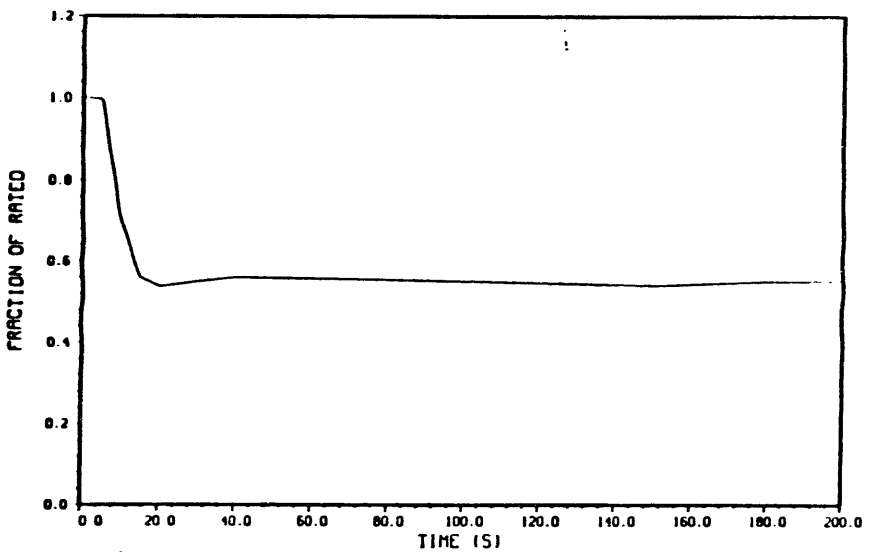

Figure 18. Feedwater Flow Boundary Condition.

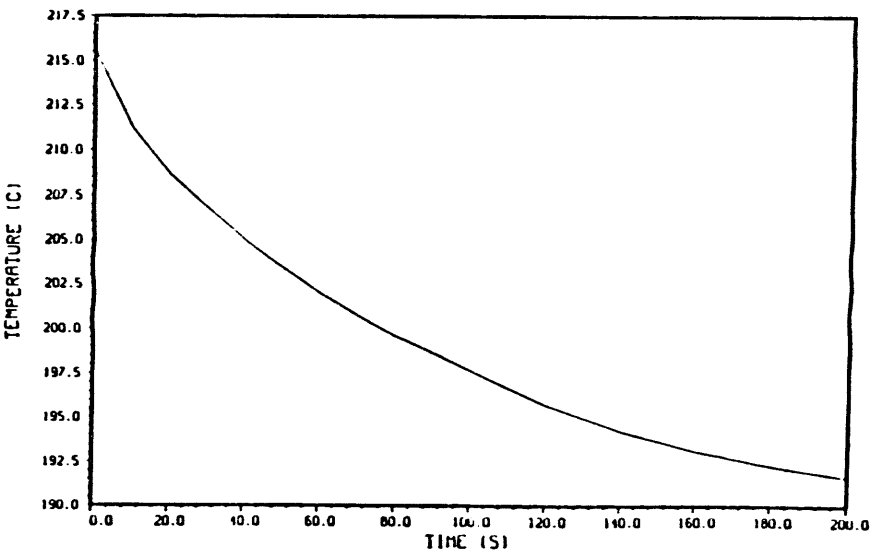

Figure 19. Feedwater Temperature Boundary Condition.

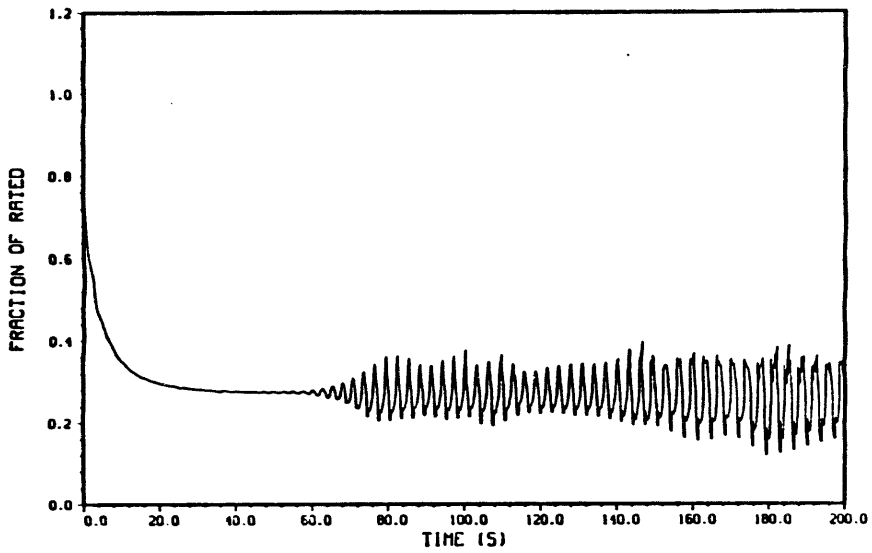

Figure 20. Total Core Inlet Flow Response During the RPT.

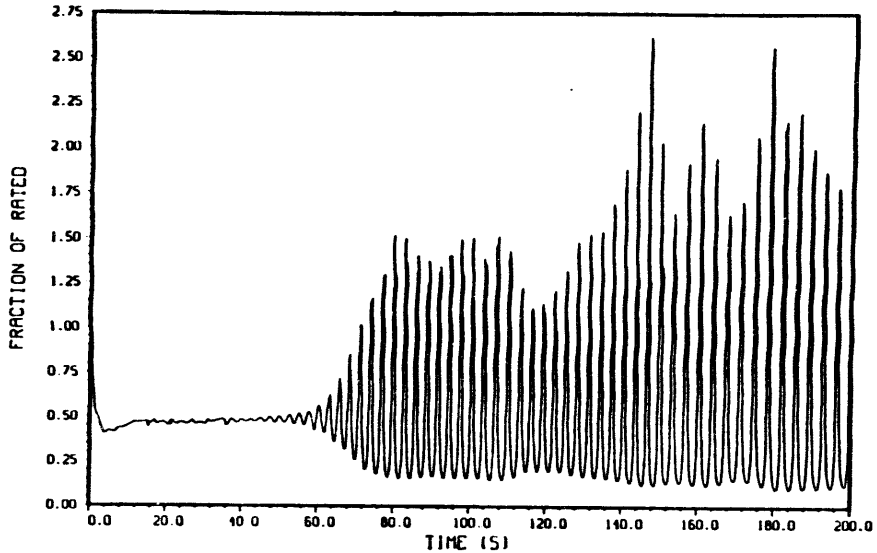

Figure 21. Core Power Response During the RPT.

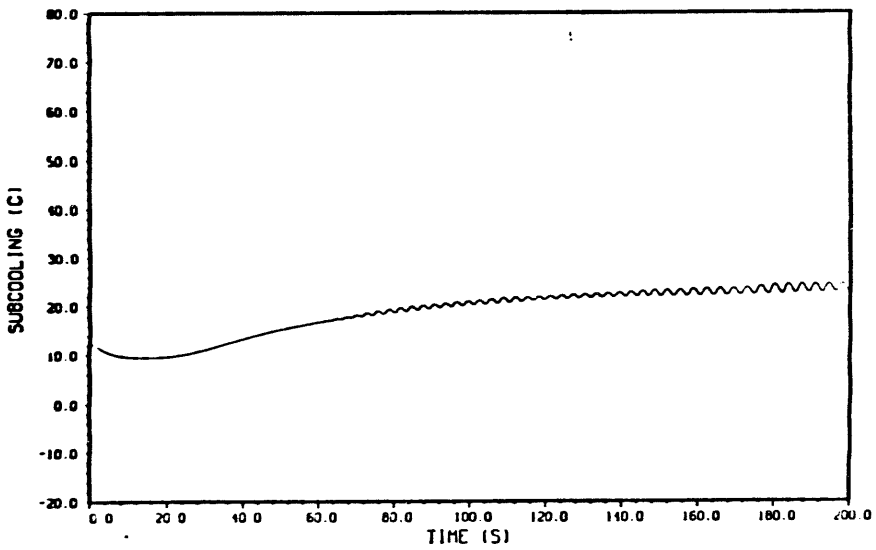

Figure 22. Core Inlet Subcooling During the RPT.

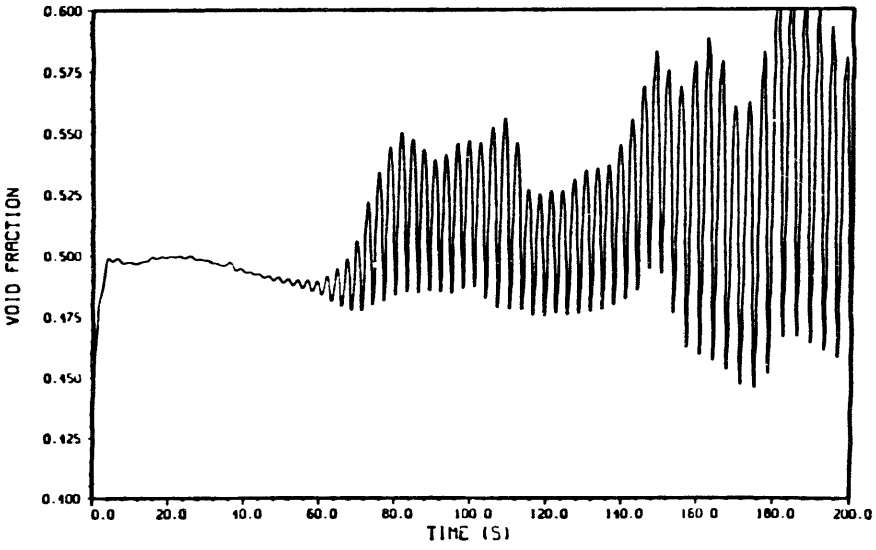

Figure 23. Core Average Void Fraction Response During the RPT.

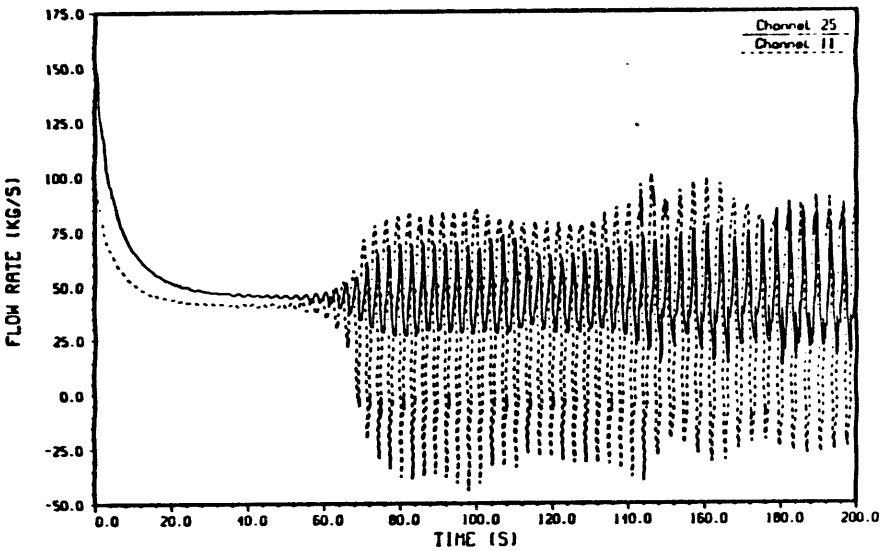

Figure 24. Individual Channel Flow Response During the RPT.

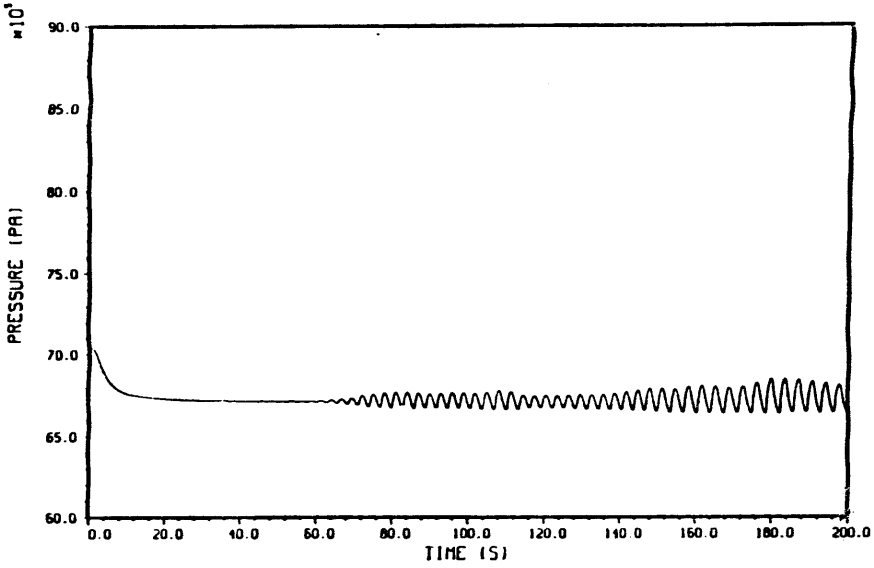

Figure 25. System Pressure Response During the RPT.

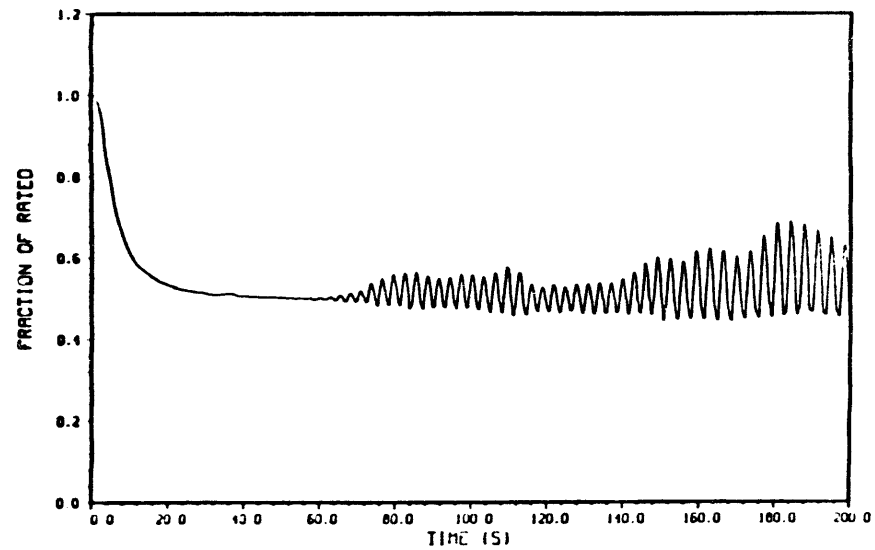

Figure 26. Steam Flow Response During the RPT.

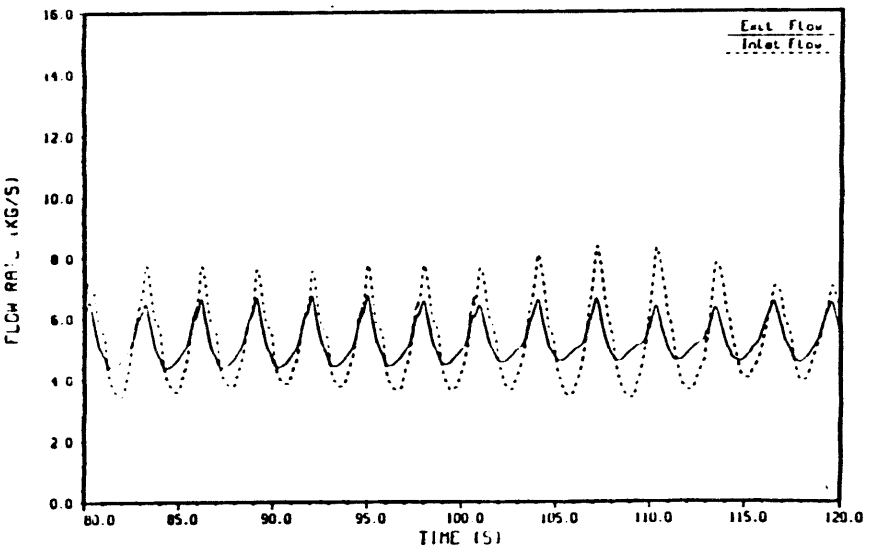

Figure 27. Channel 17, Inlet and Exit Mass Flow Rates.

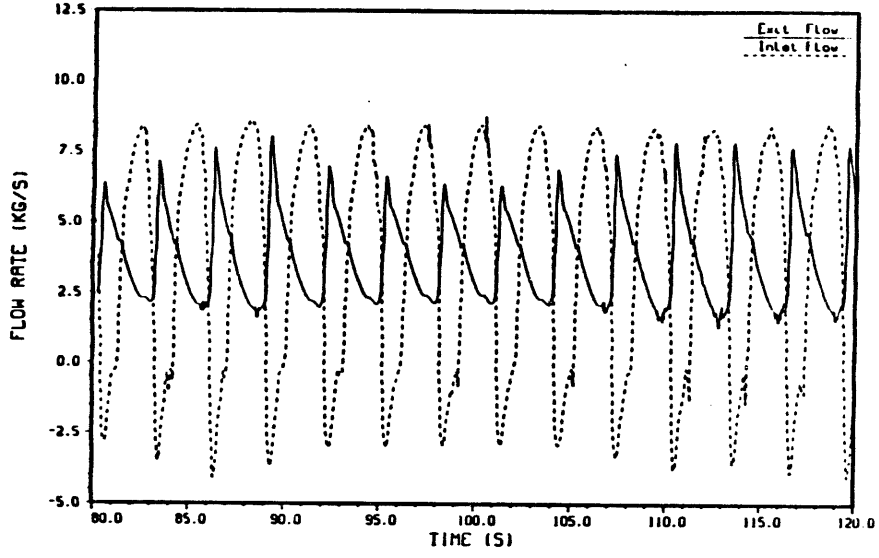

Figure 28. Channel 23, Inlet and Exit Mass Flow Rates.

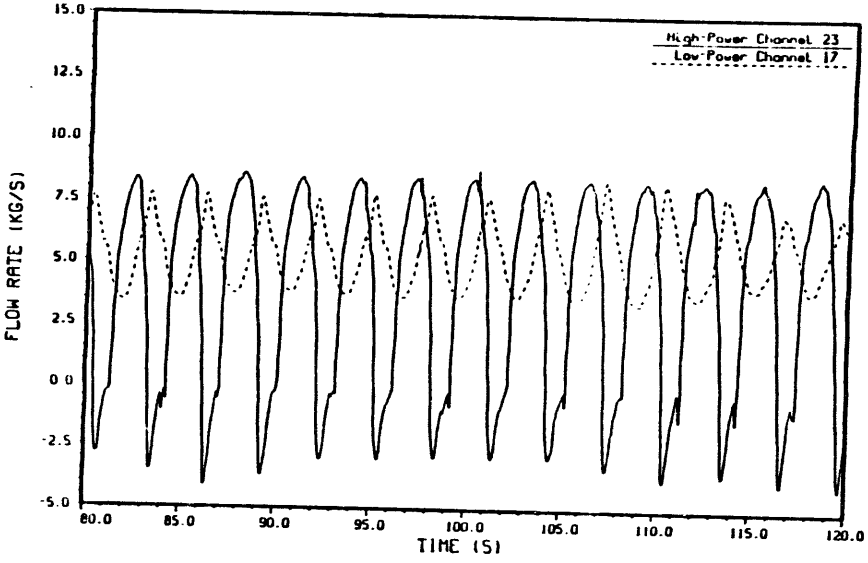

Figure 29. Inlet Flow Rates for Channel 17 and 23.

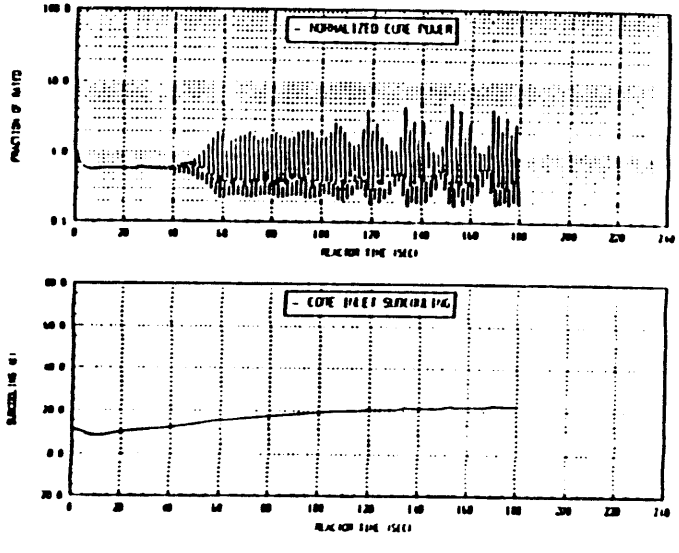

Figure 30. TRACG Results - Core Power and Inlet Subcooling.

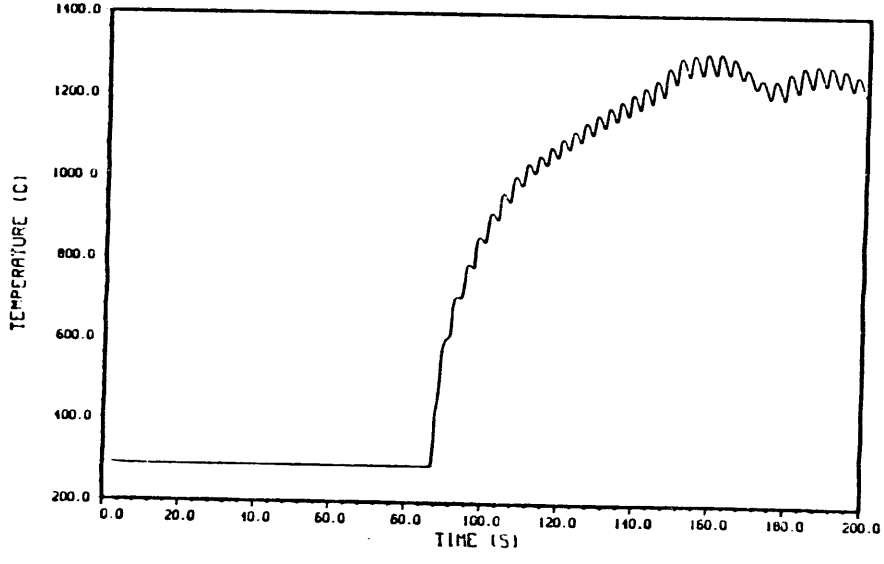

Figure 31. Peak Clad Temperature During the RPT.

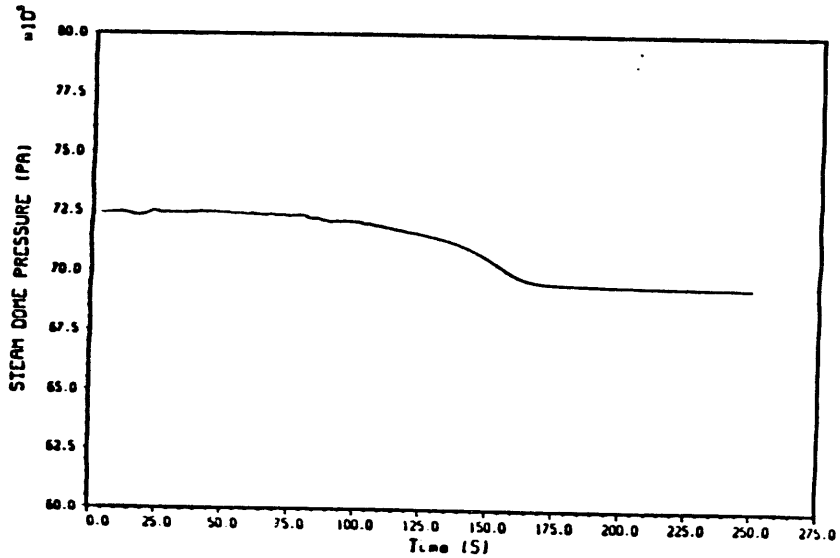

Figure 32. Pressure Profile for Loss of Feed Water Heating ATWS with Fine Motion Control Rod Insertion

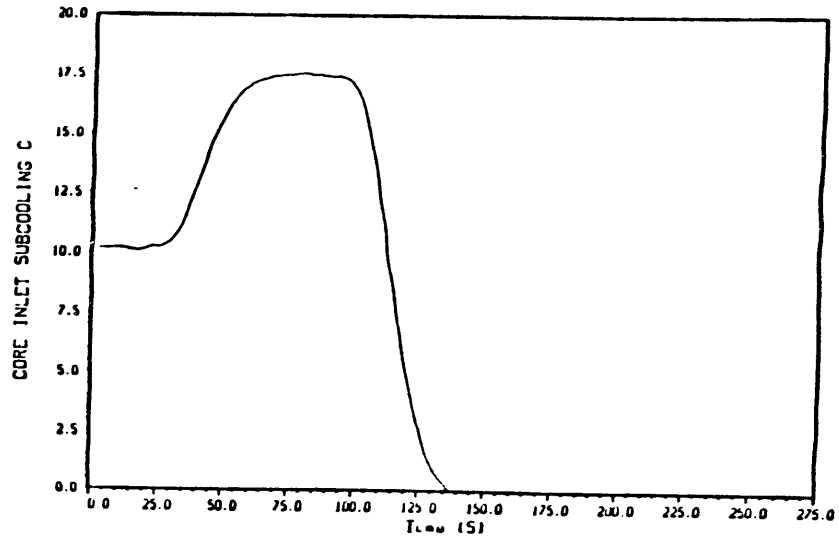

Figure 33. Inlet Subcooling for Loss of Feed Water Heating ATWS with Fine Motion Control Rod Insertion

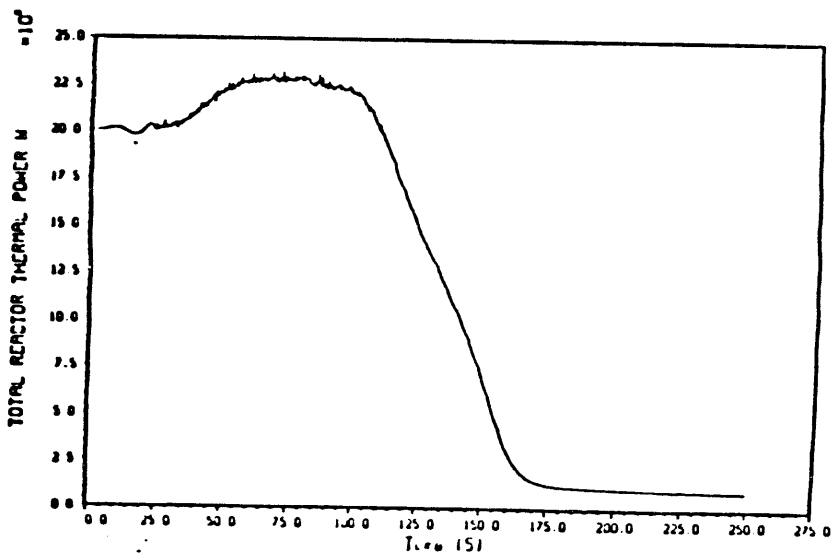

Fig. 34. Thermal Power during Loss of Feed Water Heating ATWS with Fine Motion Control Rod Insertion

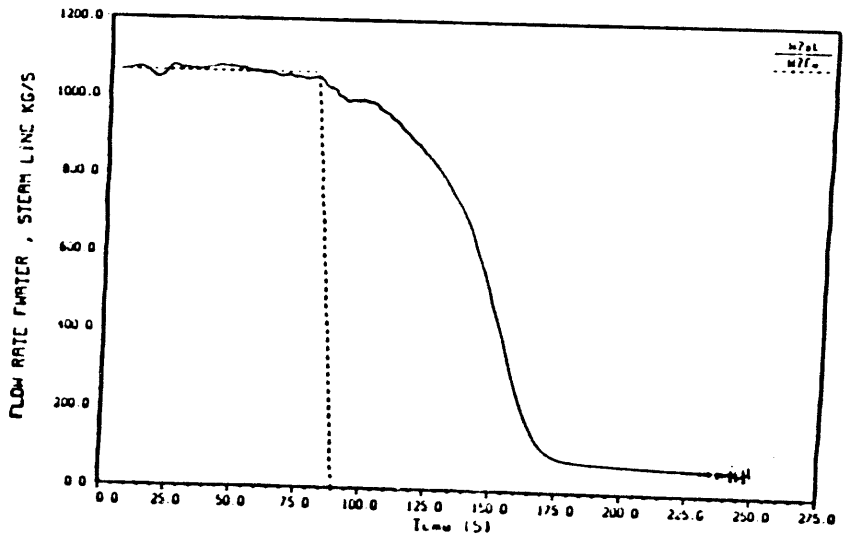

Figure 35. Feed Water and Steam Flow during Loss of Feed Water Heating ATWS with Fine Motion Control Rod Insertion

DISCLAIMER

DATE
FILMED
6/14/94
END